Realization of 70-nm T-gate InP-based PHEMT for MMW low noise applications

Wang Zhi-Ming[1a)]**, Lv Xin**[1]**, Hu Zhi-Fu**[2]**, Luo Xiao-Bin**[1]**, Cui Yu-Xing**[2]**, Sun Xi-Guo**[2]**, Mo Jiang-Hui**[2]**, and Fu Xing-Chang**[2]

[1] *Beijing Key Laboratory of Millimeter Wave and Terahertz Technology, Beijing Institute of Technology, Beijing 100081, China*

[2] *National Key Laboratory of Application Specific Integrated Circuit (ASIC), Hebei Semiconductor Research Institute, Shijiazhuang 050051, China*

a) *wangzhiming872@163.com*

Abstract: 70-nm T-gate InP-based low noise $In_{0.52}Al_{0.48}As/In_{0.65}Ga_{0.35}As$ pseudomorphic high electron mobility transistor (PHEMT) with well-balanced cutoff frequency f_t and maximum oscillation frequency f_{max} were designed and fabricated. DC, RF, and noise characterizations are demonstrated. The maximum saturation current density I_{dss} and maximum extrinsic transconductance $g_{m,max}$ are measured to be 894 mA/mm and 1640 mS/mm, respectively. And the extrapolated f_t and f_{max} based on inflection point were 247 GHz and 392 GHz, respectively. Due to the disadvantages of traditionally used *Y*-factor method, the new cold-source method was adopted to measure the noise parameters. The minimum noise figure (NF_{min}) is 1 dB at 30 GHz associated with a gain of 15 dB at V_{ds} of 0.8 V and I_{ds} of 17 mA. These excellent results make this InP-based PHEMT one of the most suitable devices for millimeter wave low noise applications.

Keywords: InP, PHEMTs, InAlAs/InGaAs, low noise, millimeter wave

Classification: Microwave and millimeter wave devices, circuits, and systems

References

[1] P. Leuther, A. Tessmann, M. Dammann, C. Schworer, M. Schlechtweg, M. Mikulla, R. Losch and G. Weimann: 2007 International Conference on Indium Phosphide and Related Materials (2007) 24. DOI:10.1109/ICIPRM.2007.380680

[2] A. Tessmann: IEEE J. Solid-State Circuits **40** (2005) 2070. DOI:10.1109/JSSC.2005.854591

[3] D.-H. Kim and J. A. del Alamo: IEEE Electron Device Lett. **31** (2010) 806. DOI:10.1109/LED.2010.2051133

[4] D.-H. Kim and J. A. del Alamo: IEEE Electron Device Lett. **29** (2008) 830. DOI:10.1109/LED.2008.2000794

[5] W. Deal, X. B. Mei, K. M. K. H. Leong, V. Radisic, S. Sarkozy and R. Lai: IEEE Trans. THz Sci. Technol. **1** (2011) 25. DOI:10.1109/TTHZ.2011.2159539

[6] G. Meneghesso, A. Neviani, R. Oesterholt, M. Matloubian, T. Liu, J. J. Brown, C. Canali and E. Zanoni: IEEE Trans. Electron Dev. **46** (1999) 2. DOI:10.1109/

16.737434

[7] S. R. Bahl and J. A. del Alamo: IEEE Electron Device Lett. **13** (1992) 123. DOI:10.1109/55.144979

[8] R. Grundbacher, R. Lai, M. Barsky, R. Tsai, T. Gaier, S. Weinreb, D. Dawson, J. J. Bautista, J. F. Davis, N. Erickson, T. Block and A. Oki: 14th Indium Phosphide and Related Material conference, IPRM (2002) 455. DOI:10.1109/ICIPRM.2002.1014466

[9] Y.-H. Zhong, X.-T. Wang, Y.-B. Su, Y.-X. Cao, Y.-M. Zhang, X.-Y. Liu and Z. Jin: Journal of Infrared and Millimeter Waves **32** [3] (2013) 193.

[10] Y.-H. Zhong, Y.-M. Zhang, Y.-M. Zhang, X.-T. Wang, H.-L. Lü, X.-Y. Liu and Z. Jin: Chin. Phys. B **22** (2013) 128503. DOI:10.1088/1674-1056/22/12/128503

[11] C. H. Liu, X. B. Mei, Y. C. Chou, L. S. Lee, J. M. Yang, M. Y. Nishimoto, P. H. Liu, R. To, A. Cavus, R. Tsai, M. Wojtowicz and R. Lai: 2009 Annual IEEE Compound Semiconductor Integrated Circuit Symposium (2009) 1. DOI:10.1109/csics.2009.5315662

[12] L. Liu, A. R. Alt, H. Benedickter and C. R. Bolognesi: IEEE Electron Device Lett. **33** (2012) 209. DOI:10.1109/LED.2011.2176713

[13] Y. Zhong, X. Wang, Y. Su, Y. Cao, Z. Jin, Y. Zhang and X. Liu: J. Semicond. **33** (2012) 074004. DOI:10.1088/1674-4926/33/7/074004

[14] D. Smith, G. Dambrine and J.-C. Orlhac: Proc. of the 3rd European Microwave Integrated Circuits Conference (2008) 214. DOI:10.1109/EMICC.2008.4772267

[15] Agilent Technologies: PNA-X Noise Figure FAQ [OL] (2014) http://www.home.agilent.com/agilent/editorial.jspx?cc=TW&lc=cht&ckey=2430705&nid=-536902643.898624&id=2430705.

1 Introduction

In recent years, there has been an increasing demand for MMICs beyond 100 GHz [1, 2]. Due to the excellent high frequency and low noise performance, InP-based PHEMT is considered to be a unique candidate for applications beyond 100 GHz. Many high performance InP-based PHEMTs have been reported [1, 2, 3, 4, 5].

Excellent performance can be obtained by the combination of gate size scaling, parasitics reduction, and an increase of InAs mole fraction in the channel that improves electron transport properties. However, with In-content increased, the impact ionization effects will become serious due to the decreased energy band gap E_G, which have a number of negative consequences, such as reduced breakdown voltages, increase in output conductance and Kink effects, and permanent device degradation [6]. A method of increasing the effective energy band gap $E_{G,eff}$ in the channel is to introduce energy quantization by reducing the channel thickness to dimensions comparable to the electron wavelength [6, 7].

In this paper, InAs mole fraction has been increased to 0.65, the thickness of channel was reduced to 11-nm for channel quantization, and the gate-length was reduced to 70 nm. The design, fabrication and characteristics were described.

2 Device structure and fabrication

The epitaxial wafers were grown by molecular beam epitaxy (MBE) on 3-inch semi-insulating InP (100) substrates. The layer structure is shown in Fig. 1 and

Table I. A room temperature electron mobility of 11,000 cm^2/v·s has been achieved with a sheet charge of 3E12 cm^{-2}. As shown in Fig. 1, the gate electrode is located at an offset position from the center toward the source. The structural improvement of the offset gate due to a reduction in the distance between the source and gate enhances the cut-off frequency (f_t) and the maximum stable gain (*MSG*) by minimizing the gate-to-drain capacitance (C_{gd}), as well as the source resistance (R_s). In this devices, the space of source-drain and space of source-gate were 2 µm and 0.8 µm, respectively.
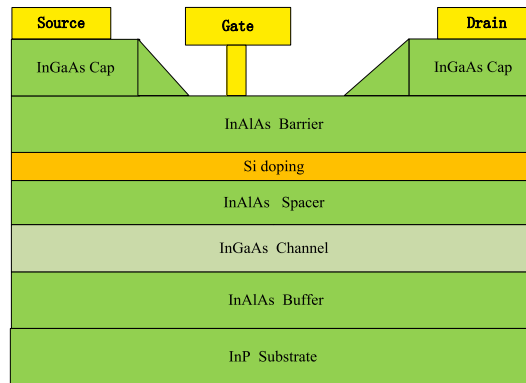

Fig. 1. InP-based PHEMT epitaxial structure

Table I. InP-based PHEMT epitaxial structure

Layer	Material	Doping	Thickness
Cap layer1	$In_{0.6}Ga_{0.4}As$	2×10^{19} cm^{-3}	10 nm
Cap layer2	$In_{0.53}Ga_{0.47}As$	5×10^{18} cm^{-3}	10 nm
Barrier layer	$In_{0.52}Al_{0.48}As$	undoped	14 nm
Si δ-doping layer		5×10^{12} cm^{-2}	
Spacer layer	$In_{0.52}Al_{0.48}As$	undoped	3 nm
Channel layer	$In_{0.65}Ga_{0.35}As$	undoped	11 nm
Buffer layer	$In_{0.52}Al_{0.48}As$	undoped	400 nm
S.I.InP Substrate (100)			

The device fabrication were based on both optical and electron beam lithography (EBL). The transistor mesa was chemically wet etched to provide isolated active areas by removing an ~200 nm thickness to expose the buffer layer, followed by the formation of ohmic contacts. The contact resistance (R_c) of 0.035 Ω·mm and the specific contact resistivity of 1.3×10^{-7} Ω·cm^{-2} were obtained by using Transmission Line Method (TLM). The gate recess was etched using a succinic acid based solution. The active devices feature T-shaped Pt-Ti-Pt-Au gates, which were defined by electron beam lithography in a three-layer resist (PMMA) process. Finally, the devices were passivated with 200-nm plasma enhanced chemical vapor deposited (PECVD) Si$_3$N$_4$ for good reliability, robustness, low leakage current and high breakdown Voltage.

3 Device performances and discussions

3.1 DC characteristics

The DC characteristics were measured by HP4142B semiconductor parameter analyzer. Fig. 2 shows the characteristics of drain current (I_{ds}) versus drain-source voltage (V_{ds}) of this device at room temperature.
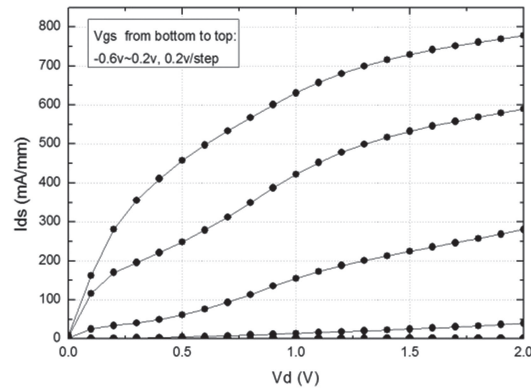

Fig. 2. DC characteristics of the device

Fig. 3 shows the characteristics of the $g_{m,max}$ and the drain current (I_{ds}) versus V_{gs} at V_{ds} of 1.5 V. The maximum g_m of the device at a V_{ds} of 1.5 V and a V_{gs} of -0.1 V was 1640 mS/mm. This high g_m is due to the superior electron transport properties in the $In_{0.65}Ga_{0.35}As$ channel and low ohmic contact resistance. A high drain current density of 894 mA/mm was observed at a V_{gs} of 0.6 V.
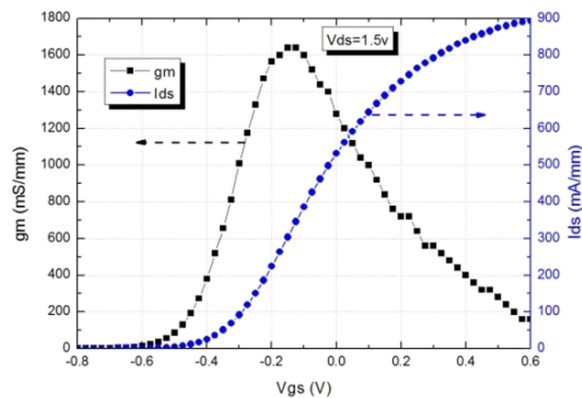

Fig. 3. I_{ds} and g_m versus V_{gs}

The off-state breakdown voltage ($BV_{off\text{-}state}$) defined at a gate current of 1 mA/mm is 3.3 V, which benefited from the 200-nm thick Si_3N_4 passivation layer and quantized channel. So the gate leakage current was very small, which was crucial for the lower frequency LNA applications since gate current was a contributing component to shot noise [8].

3.2 RF characteristics

The on-wafer RF measurements were performed by using Anritsu MS4647A series vector network analyzer and Anritsu 3743A frequency extender module

4

(70 KHz∼110 GHz) in National Institute of Metrology, China from 1 to 110 GHz with 0.5 GHz/step. And LRM (Line-Reflect-Match) method was used to calibrate the system full band from 1 to 110 GHz at a time for the first time. So the discontinuities were improved than calibrations in separate frequency bands.

The measured h_{21} gain, MAG/MSG versus the frequency were shown in Fig. 4. The current gain (H_{21}) decreases roughly with -20 dB/decade slope as the frequency increases, so the value of the $f_t = 247$ GHz was obtained by extrapolating H_{21} to 0 dB with the same slope. However, power gain MSG and MAG is related to the stability factor k of the device, when k < 1, the maximum gain is MSG which decreased with the slope of -10 dB/decade, and when k > 1, the maximum gain is MSG decreased with the slope of -20 dB/decade.
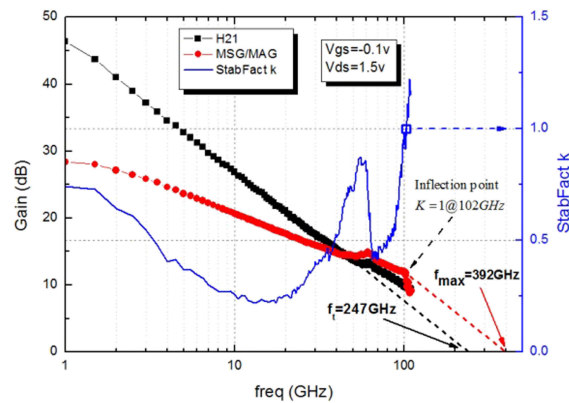

Fig. 4. Gain and the stability factor k versus frequency

As shown in Fig. 4, the inflection point (k = 1) frequency was measured to be 102 GHz, where the MAG of ∼11.7 dB was obtained, so the value of the $f_{max} = 392$ GHz was obtained by extrapolating MAG to 0 dB with -20 dB/decade slop. Thus, the extrapolated f_{max} is much more accurate than those without measured inflection point [2, 9, 10, 13]. Excellent DC and RF performances were shown in Table II.

Table II.   Comparison with published HEMTs

Reference	L_g (nm)	I_{dss} (mA/mm)	g_m (mS/mm)	f_T/f_{max} (GHz)	Test range (GHz)
[9]	150	582	1052	151/303	0∼40
[10]	150	681	952	164/390	0∼40
[11]	100	850	1150	180/-	-
[12]	100	530	700	183/230	-
[2]	100	900	1200	220/300	1∼110
[13]	88	591	765	150/201	0∼40
[14]	70	700	1600	300/300	-
[2]	50	1300	1600	380/380	1∼110
This work	70	894	1640	247/392	1∼110

3.3 Noise characteristics

An on-wafer noise parameters test is performed by using Agilent N5245A PNA-X series vector network analyzer and Maury Microwave MT984AU tuner. Due to frequency restriction of the tuner, the test frequency band is 8∼45 GHz with

0.2 GHz/step. A new cold-source method was adopted to measure the noise figure of the device. This method eliminates two large sources of error: mismatch and noise-parameter effects [15], so this technique is much more accurate than the traditionally and widely used Y-factor method.

As is shown in Fig. 5, the NF_{min} is less than 1.2 dB up to 40 GHz at V_{ds} of 0.8 V and I_{ds} of 17 mA. And as shown in Table III, an excellent NF_{min} of 1 dB is associated with a gain of 15 dB at 30 GHz.
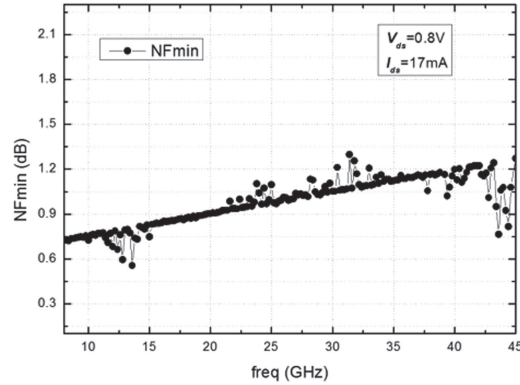

Fig. 5. NF_{min} of the device versus frequency

Table III. NF_{min} and G_{ass} Comparison with published HEMTs at 30 GHz

Reference	L_g (nm)	f_T/f_{max} (GHz)	NF_{min} (dB)	G_{ass} (dB)
[14]	130	105/105	1.1	7.5
[14]	130	150/150	0.83	11.7
[14]	70	300/300	0.55	12.8
This work	70	247/392	1	15

From the above, in this work, DC and RF performances of this device were improved basically without sacrificing noise performance, so this InP-based PHEMT is one of the best devices for millimeter wave low noise applications.

4   Conclusion

70-nm InP-based PHEMTs have been designed and fabricated. Due to the scaling gate size and the high Indium composition in the channel, good performances have been achieved, including I_{dss} of 894 mA/mm, $g_{m,max}$ of 1640 mS/mm, f_t and f_{max} of 247 GHz and 392 GHz, respectively. The NF_{min} is 1 dB with associated gain of 15 dB at 30 GHz and less than 1.2 dB up to 40 GHz. These excellent performances make this device suitable for millimeter-wave low noise applications.

Acknowledgements